

# A Combined Steepest Descent-Fast Multipole Algorithm for the Fast Analysis of Three-Dimensional Scattering by Rough Surfaces

Vikram Jandhyala, *Student Member, IEEE*, Eric Michielssen, *Member, IEEE*,  
Shanker Balasubramaniam, *Member, IEEE*, and Weng Cho Chew, *Fellow, IEEE*

**Abstract**—A new technique, the steepest descent-fast multipole method (SDFMM), is developed to efficiently analyze scattering from perfectly conducting random rough surfaces. Unlike other prevailing methods, this algorithm has linear computational complexity and memory requirements, making it a suitable candidate for analyzing scattering from large rough surfaces as well as for carrying out Monte Carlo simulations. The method exploits the quasiplanar nature of rough surfaces to efficiently evaluate the dyadic Green's function for multiple source and observation points. This is achieved through a combination of a Sommerfeld steepest descent integral and a multilevel fast multipole-like algorithm based on inhomogeneous plane wave expansions. The fast evaluation of the dyadic Green's function dramatically speeds up the iterative solution of the integral equation for rough surface scattering. Several numerical examples are presented to demonstrate the efficacy and accuracy of the method in analyzing scattering from extremely large finite rough surfaces.

**Index Terms**—Fast-multipole methods, integral equations, multilevel algorithms, rough surface scattering.

## I. INTRODUCTION

THE SCATTERING of electromagnetic waves by random rough surfaces is a subject of great practical and intellectual interest [1]. Applications [2] include, but are not limited to, remote sensing, long-range communications, radio astronomy, biomedicine, and surface physics. Random surfaces also exhibit several interesting scattering and polarization [3] characteristics. Primary among these are backscattering enhancement [4], [5] and the generation of localized modes [6], [7].

Several analytical and numerical techniques have been developed for the efficient analysis of scattering by one- and two-dimensional (1-D and 2-D) rough surfaces, which constitute 2-D and three-dimensional (3-D) scattering problems, respectively. Two well-known analytical approaches are the small perturbation method and the Kirchhoff technique [8]. Other approximate analytic methods include full-wave meth-

ods [9]–[14], a general perturbative full-wave solution [15], the small slope approximation [16], and a differential method [17]. A detailed bibliography of early analytic approaches, interesting applications, as well as experimental studies can be found in [1] and [18]–[21]. Since most of the analytic techniques have restricted regions of validity in terms of slope and roughness of the surface and are computationally very inefficient, often requiring the evaluation of many multidimensional integrals, several rigorous numerical techniques have been proposed. Of these, integral equation methods are probably the most prevalent, although the finite difference time domain method [22], [23] and direct fast solvers [24] have been used as well.

A host of integral equation techniques are available for analyzing scattering from 1-D rough surfaces. The magnetic field integral equation (MFIE) [25] has been solved using the conjugate gradient (CG) method. Other iterative techniques have also been utilized and their performances compared in [26]. Another approach to modeling rough surfaces involves a periodic-surface method of moments (MoM) formulation [27]. In order to analyze large aperiodic surfaces, fast techniques are required to accelerate the solution of the MoM system. The banded matrix iterative algorithm-fast Fourier transform (BMIA-FFT) is an interesting multilevel algorithm that accelerates matrix-vector products in the iterative solution of the MoM system and has been applied to the Monte Carlo simulation of scattering from 1-D surfaces [28], [29]. A different approach for expediting the solution of the MFIE for rough surfaces involves a particular splitting of the propagator matrix that leads to the formation of a new second-kind equation [30] that lends itself to a more efficient solution. Another MoM-based technique utilizes image theory to model inhomogeneities in a composite rough surface [31].

The analysis of 3-D scattering from 2-D rough surfaces is a complex vector problem that requires more involved numerical techniques. For large rough surfaces, solution of the MoM system using direct inversion is practically impossible due to CPU time and memory constraints. One popular approach uses the Neumann–Liouville iteration to solve the MFIE [32], [33]. In general, the iterative solution of the MoM system arising from an integral equation formulation of the 3-D problem is a time-consuming process, with both the number of operations per iteration and the memory to store the matrix scaling as  $O(N^2)$ , where  $N$  is the dimension of the system. The dense

Manuscript received April 8, 1997; revised August 27, 1997.

V. Jandhyala was with the Center for Computational Electromagnetics, Department of Electrical and Computer Engineering, University of Illinois at Urbana-Champaign, Urbana, IL 61801 USA. He is now with Ansoft Corporation, Pittsburgh, PA 15219 USA (e-mail: vikram@ansoft.com).

E. Michielssen, S. Balasubramaniam, and W. C. Chew are with the Center for Computational Electromagnetics, Department of Electrical and Computer Engineering, University of Illinois at Urbana-Champaign, Urbana, IL 61801 USA (e-mail: michiels@decwa.ece.uiuc.edu).

Publisher Item Identifier S 0196-2892(98)01143-7.

matrix representing the discretized Green's function kernel has an underlying structure that can be exploited to expedite the computation of the matrix-vector product. As succinctly stated in [34] and [35], "nature does not just throw numbers at us." The redundancy in these matrices has been exploited by several researchers to derive powerful complexity-reducing fast multipole methods (FMM's) [36]–[39] and related multilevel algorithms [40], [41] for the low-frequency regime. Substantially more complex FMM-based techniques [42]–[49] and related multilevel methods [50]–[53] have also been developed for wave scattering problems. All of these techniques compute only a small portion of the MoM matrix directly and accelerate the computation of a matrix-vector product by efficiently computing the contribution to the product from the remainder of the MoM matrix in an indirect manner.

Two extremely efficient multilevel techniques have been tailored specifically toward rough surface analysis. These methods take advantage of the fact that rough surfaces are "nearly" planar (or *quasiplanar*) to alleviate the CPU time and memory burden. The first of these techniques is the sparse matrix flat surface iterative approach (SMFSIA) [54], which is a generalization of the BMIA-FFT [28], [29] method to 2-D surfaces. In this approach, a Taylor series expansion in the vertical direction maps the problem to a flat 2-D surface. The FFT can deal efficiently with the Toeplitz structure of the interaction matrix on the flat surface. The resulting complexity of the SMFSIA is  $O(N \log(N))$ . The second approach is based on combining the FMM with the FFT [21]. The FFT is utilized in conjunction with the FMM by forcing multipole-expansion centers to lie on a 3-D separable Cartesian grid. The FFT permits the computation of the matrix-vector product in an efficient manner. The resulting algorithm, termed FMM-FFT, requires  $O(N \log(N))$  CPU time per iteration.

In this paper, a new technique, the steepest descent-fast multipole method (SDFMM) is developed for the fast analysis of 3-D scattering from 2-D perfectly conducting rough surfaces. The quasiplanar nature of rough surfaces is exploited to efficiently express the free-space dyadic Green's function in terms of a rapidly converging Sommerfeld steepest descent integral. Furthermore, the Hankel function arising in the integrand is evaluated efficiently for multiple source and observation points using a multilevel FMM-like algorithm based on an inhomogeneous plane wave expansion. Efficient and robust numerical integration rules are developed to compute the steepest descent integral arising in conjunction with the multilevel FMM. A complexity analysis is carried out to show that the proposed technique has  $O(N)$  CPU time and storage requirements. The technique is numerically rigorous and its accuracy can be controlled and traded off for computational efficiency. Several numerical examples are shown to exhibit the accuracy and efficiency of the SDFMM.

This paper is organized as follows. Section II describes rough surface modeling and the integral equation formulation of the scattering problem. In Section III, the theoretical formulation of the SDFMM method is developed. Implementation details of SDFMM interpolation and integration rules are described in Section IV. Rigorous complexity and memory estimates for the SDFMM are developed in Section V. Nu-

merical simulation results are presented in Section VI, and Section VII contains our conclusions.

## II. RANDOM ROUGH SURFACES: MODEL DEVELOPMENT AND FORMULATION OF THE SCATTERING PROBLEM

This paper focuses on scattering from Gaussian surfaces. These surfaces are chosen solely for illustration purposes as the proposed SDFMM technique is applicable to arbitrary quasiplanar scatterers (those whose lateral dimensions are much larger than their longitudinal extent). Random rough surfaces with a Gaussian distribution are generated in a two-step process [21], [32]. An uncorrelated Gaussian distribution is obtained on a discrete 2-D regular grid and then filtered in the spectral domain using a Gaussian filter. The parameters associated with this process are the variance  $\sigma$  of the zero-mean Gaussian generator and the correlation length  $l_c$  of the filter. The resulting rough surface height  $z(x, y)$  follows the statistics

$$\langle z(x, y) \rangle = 0 \quad (1a)$$

$$\langle z(x, y)z(x', y') \rangle = \sigma^2 e^{-[(x-x')^2 + (y-y')^2]/l_c^2} \quad (1b)$$

where  $\langle \cdot \rangle$  denotes an ensemble average.

In order to analyze scattering from these Gaussian surfaces, a finite sample surface  $S$  of dimensions  $L \times L$  centered at the origin is considered. The illumination on the surface should be spatially limited to avoid undesired edge effects when using such finite surfaces to model essentially infinite ones. To this end, a Gaussian-weighted sum of plane waves [21], [32] is utilized as the excitation

$$\begin{aligned} \mathbf{E}_{\text{inc}}(\mathbf{r}) &= \frac{2\pi W^2}{L^2} \\ &\times \sum_{|\mathbf{K}| \leq k_0} \hat{\mathbf{e}}_{\text{inc}}(\mathbf{K}) e^{i\mathbf{K} \cdot \mathbf{r}} e^{-ik_z z} e^{-|\mathbf{K} - \mathbf{K}_0|^2 W^2 / 2} \end{aligned} \quad (2)$$

where

$$\hat{\mathbf{e}}_{\text{inc}}(K_x, K_y, k_z) = \frac{1}{\sqrt{K_x^2 + k_z^2}} [k_z, 0, K_x] \quad (3)$$

with  $\mathbf{K}_0 = (K_{0x}, 0)$ . Also,  $W$  is the half-width of the beam and typically equals  $L/4$ .

An electric field integral equation (EFIE) is utilized to find the field scattered by the surface  $S$  when excited by  $\mathbf{E}_{\text{inc}}(\mathbf{r})$

$$\hat{\mathbf{t}} \cdot \mathbf{E}_{\text{scat}}(\mathbf{r}, \mathbf{J}) = -\hat{\mathbf{t}} \cdot \mathbf{E}_{\text{inc}}(\mathbf{r}), \quad \mathbf{r}, \mathbf{r}' \in S \quad (4a)$$

where  $\mathbf{E}_{\text{scat}}(\mathbf{r}, \mathbf{J})$  represents the scattered field generated by the surface currents  $\mathbf{J}$  and can be expressed as

$$\mathbf{E}_{\text{scat}}(\mathbf{r}, \mathbf{J}) = \frac{k_0 \eta_0}{i} \int_S \bar{\mathbf{G}}(\mathbf{r}, \mathbf{r}') \cdot \mathbf{J}(\mathbf{r}') dS', \quad \mathbf{r} \in S. \quad (4b)$$

In this equation,  $k_0$  and  $\eta_0$  are the free-space wavenumber and impedance and  $\bar{\mathbf{G}}(\mathbf{r}, \mathbf{r}')$  is the dyadic Green's function given by

$$\bar{\mathbf{G}}(\mathbf{r}, \mathbf{r}') = \left[ \bar{\mathbf{I}} + \frac{1}{k_0^2} \nabla \nabla \right] \frac{e^{ik_0 |\mathbf{r} - \mathbf{r}'|}}{4\pi |\mathbf{r} - \mathbf{r}'|} \quad (4c)$$

with  $\bar{\mathbf{I}}$  being the identity dyadic. The solution of the EFIE yields the current density  $\mathbf{J}$ , which can be used to evaluate the scattered field  $\mathbf{E}_{\text{scat}}(\mathbf{r}, \mathbf{J})$  required in the computation of the bistatic radar cross section (RCS), defined as

$$\sigma_{\alpha\beta}(\theta, \phi) = \lim_{r \rightarrow \infty} \frac{4\pi r^2 S_{\beta}(\mathbf{r})}{P_{\alpha}^{\text{inc}}} \quad (5)$$

where  $P_{\alpha}^{\text{inc}}$  is the incident beam power,  $S_{\beta}(\mathbf{r})$  is the scattered power density, and  $\alpha$  and  $\beta$  denote the polarization of the incident beam and the measured component of the scattered field, respectively. In a Monte Carlo simulation, the variance of  $\mathbf{E}_{\text{scat}}(\mathbf{r}, \mathbf{J})$  over several rough surfaces of the same root-mean-square (RMS) height is used to compute the noncoherent part of the bistatic scattering coefficient [2], [21], [33].

### III. SDFMM

To solve the EFIE (4), the unknown current density  $\mathbf{J}$  is approximated in terms of a linear combination of basic functions  $\mathbf{j}_n, n = 1, \dots, N$  as

$$\mathbf{J}(\mathbf{r}') \cong \sum_{n=1}^N I_n \mathbf{j}_n(\mathbf{r}'). \quad (6a)$$

Substituting (4b), (4c), and (6a) into (4a) and testing the resulting equation with functions  $\mathbf{f}_m, m = 1, \dots, N$ , results in a system of equations

$$\bar{\mathbf{Z}} \cdot \mathbf{I} = \mathbf{V} \quad (6b)$$

where  $\mathbf{I}$  represents the vector of unknown coefficients  $I_n$

$$Z_{mn} = \langle \mathbf{f}_m, \mathbf{E}_{\text{scat}}(\mathbf{r}, \mathbf{j}_n) \rangle \quad (6c)$$

$$V_m = \langle \mathbf{f}_m, \mathbf{E}_{\text{inc}}(\mathbf{r}) \rangle \quad (6d)$$

and  $\langle \cdot, \cdot \rangle$  denotes surface integration. A popular choice for the functions  $\mathbf{j}_n$  and  $\mathbf{f}_m$  is the Rao–Wilton–Glisson (RWG) basis [55], which will be utilized here.

Solving the matrix equation using a direct solver, such as LU decomposition, requires  $O(N^3)$  CPU time and  $O(N^2)$  memory, while Krylov subspace iterative solvers, such as those based on the CG [56] or biconjugate gradient (BiCG) [57], [58] techniques, take  $O(N^2)$  memory and CPU time per iteration. For rough surfaces, the SMFSIA [54] and FMM-FFT [21] algorithms perform matrix-vector products with  $O(N \log N)$  complexity since both approaches use FFT's as a part of their formulation. In the rest of this section, the new  $O(N)$  SDFMM algorithm (CPU time and memory) based on a hybrid Sommerfeld integral-fast multipole approach, is presented.

A single-level implementation of the SDFMM proceeds very much like that of a standard FMM by embedding the rough surface into a block of dimensions  $L \times L \times H$ , where  $H = 2\max(|z(x, y)|)$  and by partitioning this block into smaller blocks of dimensions  $l \times l \times H$  (Fig. 1). Since  $H \ll L$ , it is assumed that the block is never partitioned along the  $z$ -direction. Furthermore, since  $\langle z(x, y) \rangle = 0$ , all block centers reside in the  $x$ - $y$  plane. Based upon this partitioning, a matrix element is termed a near-field element if the corresponding basis and testing function reside in blocks that are separated by no more than  $B_{\text{di}}$  blocks in both lateral directions. (see

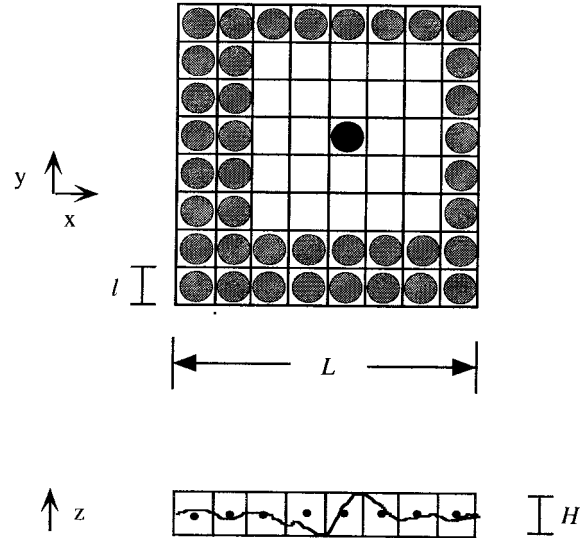


Fig. 1. SDFMM far-field interactions in a single-level implementation. The rough surface of size  $L \times L$  has been divided into blocks of dimensions  $l \times l$  centered in the  $x$ - $y$  plane. There are a total of  $b = 64$  blocks. In this example, blocks are termed well separated if they are  $B_{\text{di}} = 2$  blocks apart. Circles represent inhomogeneous plane wave expansions. The block with its expansion shown as a black circle is in the far-field of blocks whose expansions are represented by gray circles. The maximum peak-to-peak height of the rough surface is  $H$ , as shown. Centroids of all blocks are represented by small dark circles.

Fig. 1). Matrix elements that do not adhere to this definition are termed far-field elements.

The impedance matrix is decomposed as

$$\bar{\mathbf{Z}} = \bar{\mathbf{Z}}' + \bar{\mathbf{Z}}'' \quad (7)$$

where  $\bar{\mathbf{Z}}'$  and  $\bar{\mathbf{Z}}''$  contain all near-field and far-field interactions, respectively. In the SDFMM, the matrix  $\bar{\mathbf{Z}}'$  is computed and stored as in the regular MoM. However,  $\bar{\mathbf{Z}}''$  is never computed since an efficient representation of  $\bar{\mathbf{Z}}''$  can be obtained upon representing  $\bar{\mathbf{G}}(\mathbf{r}, \mathbf{r}')$  using a diagonalized translation operator. To arrive at this new representation of  $\bar{\mathbf{Z}}''$ , consider two points  $\mathbf{r}$  and  $\mathbf{r}'$  residing in each other's far-field. The 3-D dynamic scalar Green's function

$$g(\mathbf{r}, \mathbf{r}') = \frac{e^{ik_0|\mathbf{r}-\mathbf{r}'|}}{4\pi|\mathbf{r}-\mathbf{r}'|} \quad (8)$$

can be cast into a contour integral form [59] using the Sommerfeld identity

$$\frac{e^{ik_0|\mathbf{r}-\mathbf{r}'|}}{4\pi|\mathbf{r}-\mathbf{r}'|} = \frac{i}{8\pi} \int_{-\infty}^{\infty} dk_z e^{ik_z(z-z')} H_0^{(1)}(k_\rho|\rho-\rho'|) \quad (9)$$

where  $z, z'$  and  $\rho, \rho'$  are the cylindrical coordinate representation of  $\mathbf{r}, \mathbf{r}'$ . We seek to approximate the above integral numerically by using quadrature rules. This is most expediently performed along the steepest descent path (SDP) when  $|\rho-\rho'|$  is large. To this end, we let

$$H_0^{(1)}(k_\rho|\rho-\rho'|) = \hat{H}_0^{(1)}(k_\rho|\rho-\rho'|) e^{ik_\rho|\rho-\rho'|} \quad (10)$$

so that  $\hat{H}_0^{(1)}(x)$  is a nonoscillating function when  $x$  is large. Then

$$g(\mathbf{r}, \mathbf{r}') = \frac{i}{8\pi} \int_{-\infty}^{\infty} dk_z e^{ik_z(z-z')} \hat{H}_0^{(1)}(k_\rho |\boldsymbol{\rho} - \boldsymbol{\rho}'|) e^{ik_\rho |\boldsymbol{\rho} - \boldsymbol{\rho}'|}. \quad (11)$$

By letting  $k_z = k_0 \cos \alpha$ ,  $k_\rho = k_0 \sin \alpha$ , the above becomes

$$g(\mathbf{r}, \mathbf{r}') = -\frac{ik_0}{8\pi} \int_{\Gamma} d\alpha \sin \alpha \hat{H}_0^{(1)} \times (k_0 \sin \alpha |\boldsymbol{\rho} - \boldsymbol{\rho}'|) e^{ik_0 |\mathbf{r} - \mathbf{r}'| \cos(\alpha - \theta)} \quad (12)$$

where  $\theta = \tan^{-1}(|\boldsymbol{\rho} - \boldsymbol{\rho}'|/(z - z'))$ . The saddle point is at  $\alpha = \theta$ . However, since  $\theta \approx \pi/2$  for a quasiplanar structure, we evaluate the integral along an approximate SDP through  $\alpha = \pi/2$  defined by

$$ik_0 |\boldsymbol{\rho} - \boldsymbol{\rho}'| \cos(\alpha - \pi/2) = ik_0 |\boldsymbol{\rho} - \boldsymbol{\rho}'| - s^2 \quad (13)$$

since this path can be used as a common one for all sources and observers residing in any of the blocks. Upon deforming the integrand along the SDP, we obtain

$$g(\mathbf{r}, \mathbf{r}') = -\frac{ik_0}{8\pi} e^{ik_0 |\boldsymbol{\rho} - \boldsymbol{\rho}'|} \int_{-\infty}^{\infty} ds \frac{d\alpha}{ds} \sin \alpha \hat{H}_0^{(1)} \times (k_0 \sin \alpha |\boldsymbol{\rho} - \boldsymbol{\rho}'|) e^{-s^2} e^{ik_z(z-z')}. \quad (14)$$

Efficient quadrature rules can be developed for computing the above integral, with the number of points  $n_{\text{sd}}$  determined by the exponential decay in the integrand and the phase variation, governed in turn by  $|z' - z|$ . These rules are developed and examined in Section IV. Using such a rule, the above integral can be approximated as

$$g(\mathbf{r}, \mathbf{r}') = \frac{i}{8\pi} e^{ik_0 |\boldsymbol{\rho} - \boldsymbol{\rho}'|} \sum_{j=1}^{n_{\text{sd}}} w_j^{\text{sd}} k_\rho^{(j)} \hat{H}_0^{(1)} \times (k_\rho^{(j)} |\boldsymbol{\rho} - \boldsymbol{\rho}'|) e^{-s_j^2} e^{ik_z^{(j)}(z-z')} \quad (15)$$

where  $k_\rho^{(j)} = k_0 \sin \alpha_j$  and since  $\alpha$  is a function of  $s$  via (13),  $\alpha_j = \alpha(s_j)$ . Numerical quadrature weights are denoted by  $w_j^{\text{sd}}$ . Using (10) and (13) in (15), we have

$$g(\mathbf{r}, \mathbf{r}') \approx \frac{i}{8\pi} \sum_{j=1}^{n_{\text{sd}}} w_j^{\text{sd}} k_\rho^{(j)} H_0^{(1)}(k_\rho^{(j)} |\boldsymbol{\rho} - \boldsymbol{\rho}'|) e^{ik_z^{(j)}(z-z')}. \quad (16)$$

The Hankel function occurring in the above integrand can be computed efficiently for several source and observation locations through a generalization of the free-space FMM [49], [34] by using the addition theorem and transforming to an inhomogeneous plane wave basis. The rough surface is divided into blocks lying on a plane. Sources lying in each block are represented by plane wave expansions located at the center of each block, irrespective of the particular  $z$  location of the

source. The Hankel function can then be expressed as

$$H_0^{(1)}(k_\rho^{(j)} |\boldsymbol{\rho} - \boldsymbol{\rho}'|) \cong \frac{1}{2\pi} \int_0^{2\pi} d\phi e^{ik_\rho^{(j)}(\boldsymbol{\rho} - \boldsymbol{\rho}_c) \cdot \hat{\mathbf{s}}} \times \mathcal{T}(k_\rho^{(j)}, \hat{\mathbf{s}}, \boldsymbol{\rho}_c - \boldsymbol{\rho}_a) e^{ik_\rho^{(j)}(\boldsymbol{\rho}_a - \boldsymbol{\rho}') \cdot \hat{\mathbf{s}}} \cong \frac{1}{2\pi} \sum_{j'=1}^P w_{j'}^{\text{fmm}} e^{ik_\rho^{(j)}(\boldsymbol{\rho} - \boldsymbol{\rho}_c) \cdot \hat{\mathbf{s}}_{j'}} \times \mathcal{T}(k_\rho^{(j)}, \hat{\mathbf{s}}_{j'}, \boldsymbol{\rho}_c - \boldsymbol{\rho}_a) e^{ik_\rho^{(j)}(\boldsymbol{\rho}_a - \boldsymbol{\rho}') \cdot \hat{\mathbf{s}}_{j'}} \quad (17a)$$

$$\mathbf{k}^{(j)} = k_\rho^{(j)} \hat{\boldsymbol{\rho}} + k_z^{(j)} \hat{\mathbf{z}} \quad (17b)$$

where

$$\mathcal{T}(k_\rho^{(j)}, \hat{\mathbf{s}}, \boldsymbol{\rho}_c - \boldsymbol{\rho}_a) = \sum_{p=-P}^P H_p^{(1)}(k_\rho^{(j)} |\boldsymbol{\rho}_c - \boldsymbol{\rho}_a|) \times e^{-ip[\theta - \phi - \pi/2]} \quad (17c)$$

where  $P$  is the number of integration points required for spectral integration,  $w_{j'}^{\text{fmm}}$  are the quadrature weights (typically obtained from equispaced rules on a circle [60]),  $\boldsymbol{\rho}_a$  and  $\boldsymbol{\rho}_c$  are FMM block centers, and  $\mathcal{T}$  is the translation operator that depends on the complex wavenumber, spectral angle, and the displacement between source and observation blocks. Also,  $\hat{\mathbf{s}} = \hat{\mathbf{x}} \cos \phi + \hat{\mathbf{y}} \sin \phi$ , and  $\cos \theta = \hat{\mathbf{x}} \cdot (\boldsymbol{\rho}_c - \boldsymbol{\rho}_a) / |\boldsymbol{\rho}_c - \boldsymbol{\rho}_a|$ . On using the above equation in conjunction with (4) and (16), the dyadic Green's function  $\bar{\mathbf{G}}(\mathbf{r}, \mathbf{r}')$  can be represented in the SDFMM formulation as

$$\bar{\mathbf{G}}(\mathbf{r}, \mathbf{r}') \cong \frac{i}{16\pi^2} \sum_{j=1}^{n_{\text{sd}}} \sum_{j'=1}^P w_j^{\text{sd}} w_{j'}^{\text{fmm}} k_\rho^{(j)} \times \left( \bar{\mathbf{I}} - \frac{\mathbf{k}^{(j)} \mathbf{k}^{(j)}}{k_0^2} \right) e^{i\mathbf{k}^{(j)} \cdot (\mathbf{r} - \mathbf{r}_c)} \times \mathcal{T}(k_\rho^{(j)}, \hat{\mathbf{s}}_{j'}, \boldsymbol{\rho}_c - \boldsymbol{\rho}_a) e^{i\mathbf{k}^{(j)} \cdot (\mathbf{r}_a - \mathbf{r}')} \quad (18a)$$

$$\mathbf{k}^{(j)} = k_\rho^{(j)} \hat{\boldsymbol{\rho}} + k_z^{(j)} \hat{\mathbf{z}}. \quad (18b)$$

Fig. 2 shows a schematic representation of the dyadic Green's function evaluation in the SDFMM. We conclude that, if the  $m$ th testing and  $n$ th basis functions are in each other's far-field, then from (6c),  $Z''_{mn}$  can be expressed as

$$Z''_{mn} \cong \frac{i}{16\pi^2} \sum_{j=1}^{n_{\text{sd}}} \sum_{j'=1}^P w_j^{\text{sd}} w_{j'}^{\text{fmm}} k_\rho^{(j)} \int_S d\mathbf{r} \mathbf{f}_m e^{i\mathbf{k}^{(j)} \cdot (\mathbf{r} - \mathbf{r}_c)} \times \mathcal{T}(k_\rho^{(j)}, \hat{\mathbf{s}}_{j'}, \boldsymbol{\rho}_c - \boldsymbol{\rho}_a) \left( \bar{\mathbf{I}} - \frac{\mathbf{k}^{(j)} \mathbf{k}^{(j)}}{k_0^2} \right) \times \int_S d\mathbf{r}' \mathbf{j}_n e^{i\mathbf{k}^{(j)} \cdot (\mathbf{r}_a - \mathbf{r}')}. \quad (19)$$

The inhomogeneous plane wave expansions above are amenable to aggregation and disaggregation processes analogous to those in standard FMM's, refer to [42]–[46]. The computational complexity of a matrix-vector product involving  $\bar{\mathbf{Z}}$  is substantially reduced in FMM methods by using the diagonal translation operator and by utilizing the fact that the far-field plane wave expansions can be produced

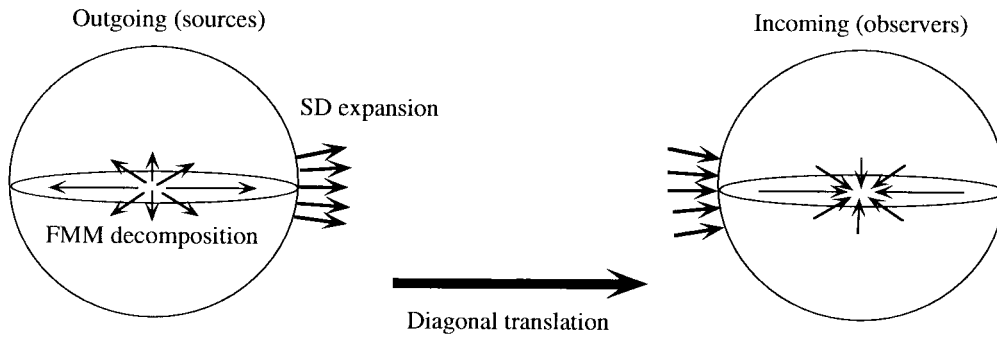


Fig. 2. Schematic SDFMM representation of the dyadic Green's function. A rough surface has been divided into blocks, and two such blocks are represented by their SDFMM expansions, shown as spheres. For each block, fields produced by sources in that block are represented by a hybrid SDFMM formulation. The SD integration is represented by the short bold arrows ( $n_{sd}$  in number), while the FMM spectral integration is shown as thinner arrows ( $P$  in number) lying on a plane. The long bold arrow represents the diagonal translation operators, translating an amount of information proportional to the product  $n_{sd}P$ . At an observation block, incoming inhomogeneous plane waves are utilized to obtain the field value at the center of the block through the use of another combined SDFMM integration.

independently, irrespective of the location of source and observer locations.

The SDFMM implementation utilizes a multilevel FMM-like algorithm for inhomogeneous plane waves analogous to existing free-space multilevel FMM's [45]. In this case, the rough surface is divided hierarchically into blocks lying in the  $x$ - $y$  plane, irrespective of the height of the rough surface, by recursively dividing each block into four smaller blocks. The block at the coarser level is termed the *parent*, and the derivative blocks are its *children*. Plane wave expansions are shifted to centers of parent blocks, and incoming spectra are shifted to centers of child blocks. Distinct translation operators are utilized at each FMM level. At the finest level, sources lying in each block are represented by plane wave expansions about the block center.

#### IV. IMPLEMENTATION DETAILS FOR SDFMM INTEGRATION AND INTERPOLATION RULES

This section examines in detail the implementation and performance of numerical integration rules for SDP integration. As will be demonstrated, these rules have to satisfy certain validity conditions in order that the integration be compatible with the use of the FMM. Specific features incorporated into the multilevel FMM are also discussed. These include the use of optimal bandlimited interpolation and the truncation of translation operators based on bandlimited windowing.

To examine the nature of the integrand in the SDP integral, we use the small argument approximation of  $\cos(\alpha - \pi/2)$  when  $\alpha \rightarrow \pi/2$  in (13), to get

$$ik_0|\rho - \rho'| \frac{(\alpha - \pi/2)^2}{2} \approx s^2. \quad (20)$$

By letting  $(1 - i)t/\sqrt{2} = \alpha - \pi/2$ , where  $t$  is real along the SDP in the vicinity of the saddle point, the overall exponent  $\phi = -s^2 + ik_z(z - z')$  in (14) has a real part defined by

$$\text{Re}(\phi) = \frac{k_0(z' - z)t}{\sqrt{2}} - \frac{k_0|\rho - \rho'|t^2}{2}. \quad (21)$$

The exponential term therefore has its largest magnitude at  $t = (z' - z)/(\sqrt{2}|\rho - \rho'|)$ . To examine the exponential decay

away from this point, a new variable  $t'$  is introduced as

$$t' = t - \frac{z' - z}{\sqrt{2}(|\rho - \rho'|)} \quad (22)$$

and therefore

$$\text{Re}(\phi) = -\frac{k_0|\rho - \rho'|t'^2}{2} + \frac{k_0(z' - z)^2}{4|\rho - \rho'|} \quad (23)$$

and the double-sided exponential decay of the integrand on either side of  $t = (z' - z)/(\sqrt{2}|\rho - \rho'|)$  is evident. The region of integration is thus restricted to a small region around this point. For multiple source and observation points, the location of the maximum will shift and the "spread" will be related to  $|z' - z|/(\sqrt{2}|\rho - \rho'|)$ . The phase variation of the integrand is mainly governed by the imaginary part of  $\phi$ , which, for small  $t$  is

$$\text{Im}(\phi) = \frac{ik_0(z' - z)t}{\sqrt{2}}. \quad (24)$$

The number of points for an integrand composing several source and observation points will be influenced by the phase variation. As  $(z' - z)$  increases, the phase varies more rapidly and more points are required in the rule. This is akin to the sampling theorem required for perfect interpolation, where a larger frequency component entails a denser sampling due to the increased Nyquist rate. The fact that one is working with a rough surface implies that  $(z' - z)$  will be small compared to the lateral dimensions of the surface, and therefore, a robust numerical integration can be performed using a small number of points.

It is tempting at first glance to utilize one of the readily available integration methods [60] for the purpose of SDP integration. Unfortunately, this approach leads to an invalid rule in the present context. Interactions between FMM blocks at a particular level are restricted to a range. Interacting blocks are those that are in each other's far-field and whose parent blocks are not [37], [42]. The SDP integration must be valid for all source-observation displacements in the interacting range. This means that a *fixed* set of integration weights  $w_j^{sd}$  (obtained from standard quadrature rules [60]) and locations  $k_{\rho}^{(j)}$  (or

TABLE I  
OPTIMAL UPPER BOUNDS ON  $|t|$  FOR NUMERICAL SDP INTEGRATION

Maximum height	$n_{sd}$	Optimal bound of $ t $
0.1	5	0.75
0.1	10	1.05
0.1	15	1.34
1.0	5	0.7
1.0	10	1.08
1.0	15	1.35
1.0	20	1.56
2.0	10	1.10
2.0	15	1.35
2.0	20	1.53
2.0	25	1.70

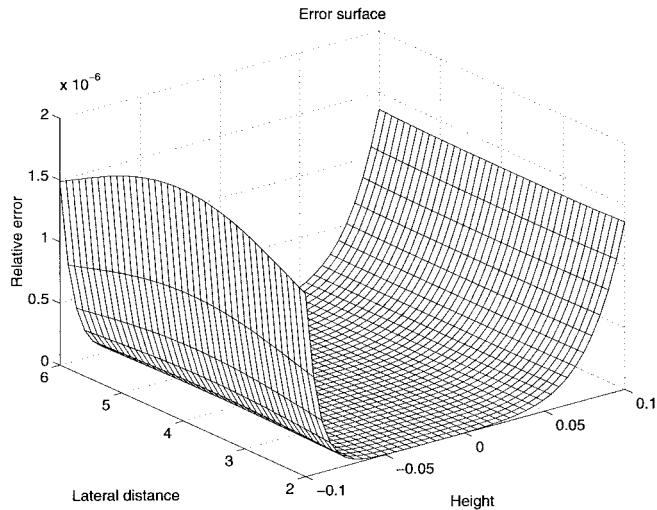


Fig. 3. Accuracy of the numerical SDP integration. The FMM block has a size of  $1\lambda \times 1\lambda$ . Lateral distances and heights are in units of  $\lambda$ .

equivalently  $k_z^{(j)}$  have to be valid for a range of  $z' - z$  and  $\rho - \rho'$  in (16), rather than simply for a single integrand.

The method used here to derive optimal equispaced rules for the above purpose is the following. The parameters to be determined are the number of points  $n_{sd}$  in the rule as well as the limit of the integration variable  $s$  in (14). It is observed that the numerical error is largest for the maximum value of  $|z' - z|$  (which is when the integrand has the greatest oscillations). Also, the range of interaction of FMM blocks at a particular level  $l$  specifies lower and upper limits on  $\rho - \rho'$ , termed  $\rho_{min,l}$  and  $\rho_{max,l}$ , respectively. The exact limit of  $s$  for integration at level  $l$  is determined in an optimal manner for a given  $n_{sd}$  by forcing the errors in integration to be identical in the cases when  $\rho - \rho' = \rho_{min,l}$  and  $\rho - \rho' = \rho_{max,l}$ . For FMM blocks

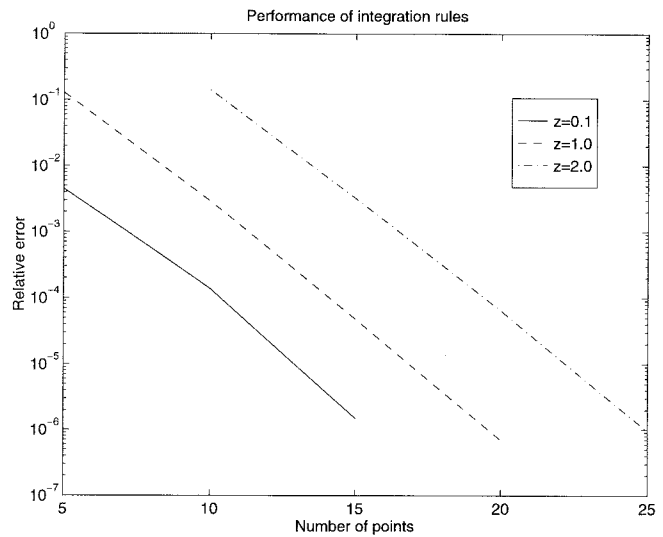


Fig. 4. Accuracy of integration rules. The FMM block has a size of  $1\lambda \times 1\lambda$ ,  $\rho_{min,l} = 2\lambda$ , and  $\rho_{max,l} = 6\lambda$ . Heights are in units of  $\lambda$ .

of size  $1\lambda \times 1\lambda$  (where  $\lambda$  denotes a free-space wavelength) and a maximum  $|z' - z|$  of  $0.1\lambda$ , the error surface generated by the suggested approach is shown in Fig. 3. As is evident, the error reduces as  $|z' - z|$  reduces and is practically independent of  $\rho - \rho'$ . In exactly the same manner, optimal equispaced rules can be developed for different FMM levels and different rough surface heights. Moreover, the number of points  $n_{sd}$  is determined by the acceptable error and is a function of the roughness. The dependence of integration error on  $n_{sd}$  and rough surface height is seen clearly in Fig. 4. The FMM block is of size  $1\lambda \times 1\lambda$ ,  $\rho_{min,l} = 2\lambda$ , and  $\rho_{max,l} = 6\lambda$ . For the same case, the optimal value of  $t$ , which minimizes the error, is a strong function of  $n_{sd}$ , as can be seen from Table I. Moreover, this optimal value is not as strongly influenced

by the height, which is what was postulated earlier in this section.

For the implementation of the multilevel FMM, interpolation rules are required to obtain sampled values of inhomogeneous plane wave spectra that are utilized at coarser FMM levels. For this purpose, optimal bandlimited interpolation [61] is utilized. In this approach, kernels based on prolate-spheroidal or Chebyshev functions are used to interpolate bandlimited functions. In the SDFMM, these same functions are also utilized as windowing functions for sparsifying the diagonalized translation operator.

## V. COMPUTATIONAL COMPLEXITY ESTIMATES FOR THE SDFMM

To analyze the computational complexity and memory requirements of the SDFMM, assume a rough surface of dimensions  $L \times L \lambda^2$ , with a maximum peak to peak height of  $H$ , modeled using  $N$  unknowns. Let the number of FMM levels be  $f$ . At any intermediate level  $g$ , the number of blocks is denoted by  $b^{(g)}$  and the size of each block is  $l^{(g)} \times l^{(g)} \lambda^2$ . Furthermore, let the number of points used for the steepest descent integration and the number of spectral angles required by the FMM be  $n_{\text{sd}}^{(g)}$  and  $P^{(g)}$ , respectively (see Figs. 1 and 2). Finally ( $g$ -independent) constants are denoted by  $C_i$ , where  $i$  is some integer. The following relations hold:

$$b^{(g)} = (L/l^{(g)})^2 \quad (25a)$$

$$l^{(g-1)} = 2l^{(g)} \quad (25b)$$

$$f = (\log_2(L/l^{(f)})). \quad (25c)$$

The upper bound  $I_d$  on the total number of near-field interactions is given by

$$I_d = (2B_{\text{di}} + 1)^2 N^2 (l^{(f)}/L)^2. \quad (26a)$$

Moreover,  $L^2 = C_1 N$  and, therefore

$$I_d = (2B_{\text{di}} + 1)^2 N (l^{(f)})^2 / C_1. \quad (26b)$$

An initial step for the computation of far-field contributions is the projection of sources, which involves computing plane wave spectra at the centers of finest level blocks. The next step is the recursive generation of higher level spectra, which involves spectrum interpolation and center translation. A dual step is the anterpolation of incoming spectra at finer levels and center translation. In-level translations using the diagonalized translation operator are also necessitated to obtain complete incoming wave spectra. At the finest level, plane wave spectra need to be backprojected to obtain actual field values. The overall far-field computation cost is calculated as follows. The total cost of projection and backprojection  $I_p$  is given by

$$I_p = C_2 n_{\text{sd}}^{(f)} P^{(f)} N. \quad (27)$$

The cost of all center translations and interpolation/anterpolation  $I_c^{(g)}$  at level  $g$  is

$$I_c^{(g)} = C_3 n_{\text{sd}}^{(g)} P^{(g)} b^{(g)} \quad (28)$$

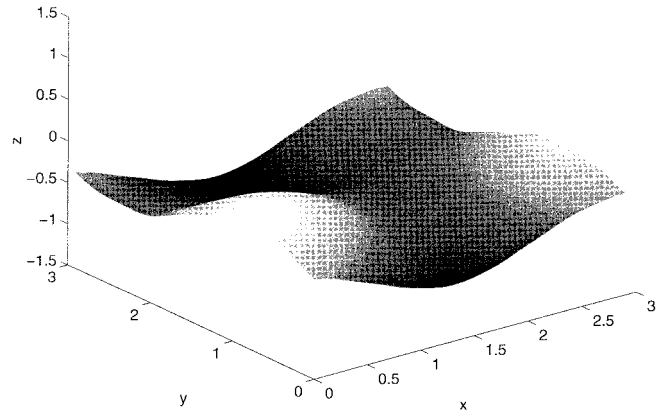


Fig. 5. Sample rough surface. All dimensions in units of  $\lambda$ .

and the cost of in-level translations  $I_t^{(g)}$  is given by

$$I_t^{(g)} = C_4 n_{\text{sd}}^{(g)} P^{(g)} (2B_{\text{di}} + 1)^2 b^{(g)}. \quad (29)$$

We can assume that  $n_{\text{sd}}^{(g)}$  is independent of the level  $g$  and, hence, equals  $n_{\text{sd}}^{(f)}$ . This is in keeping with the observations earlier in this paper, where it was shown that the number of points for steepest descent integration is dependent mainly on the rough surface height. The number of spectral angles required depends on the block size and roughly double as the block size doubles [61]. Therefore, in this complexity analysis, we let  $P^{(g)} = 2P^{(g+1)}$ . The overall cost of the SDFMM is

$$I_{\text{SDFMM}} = I_d + I_p + \sum_{g=0}^f (I_c^{(g)} + I_t^{(g)}) \quad (30a)$$

$$I_{\text{SDFMM}} = (2B_{\text{di}} + 1)^2 N (l^{(f)})^2 / C_1 + n_{\text{sd}}^{(f)} P^{(f)} N [C_5 + C_6 (2B_{\text{di}} + 1)^2] \quad (30b)$$

and, therefore

$$I_{\text{SDFMM}} = O(N). \quad (30c)$$

It is evident that the cost of each matrix-vector product is  $O(N)$  and the total memory requirements (storing near-field interactions and incoming and outgoing spectra at all levels) are also  $O(N)$ . Owing to the exponential decay characteristics of the SDP and FMM integration rules, the computational cost for a matrix-vector product is  $O(N \ln \epsilon^{-1})$  for an arbitrary and fixed error tolerance of  $\epsilon$ .

## VI. NUMERICAL RESULTS

The SDFMM has been developed in this paper to analyze scattering from random rough surfaces, although it is in principle applicable to a more general class of quasiplanar structures. In this section, results of applying the SDFMM to solve scattering problems, specifically, involving Gaussian rough surfaces are presented. Single RCS and Monte Carlo simulation results as well as CPU time and memory requirements are presented.

To validate the SDFMM approach, a comparison is made with results obtained by using the standard MoM technique. The rough surface used for this purpose, shown in Fig. 5, has a roughness  $\sigma = 0.5\lambda$  and correlation length  $l_c = 1.5\lambda$ .

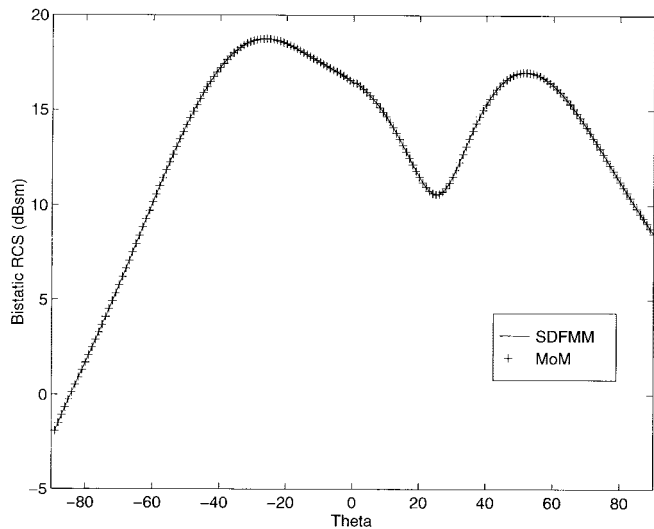


Fig. 6. Bistatic RCS: SDFMM and MoM results. A Gaussian beam is incident at  $\theta = -10^\circ$ .

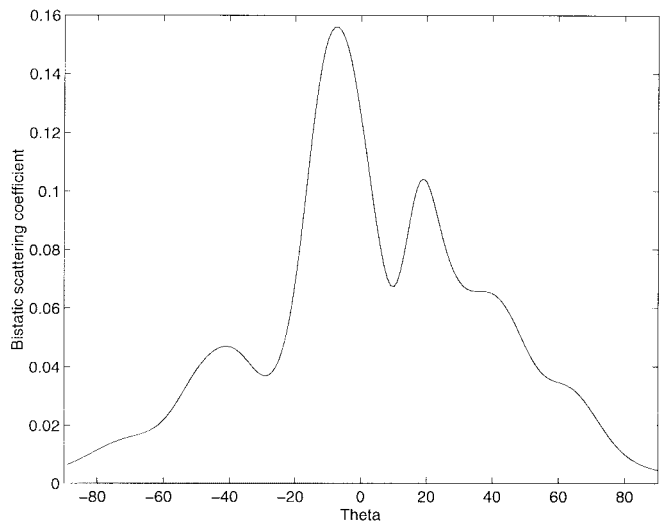


Fig. 8. Monte Carlo simulation: Cross-polarized bistatic scattering coefficient. A Gaussian beam is incident at  $\theta = -10^\circ$ .

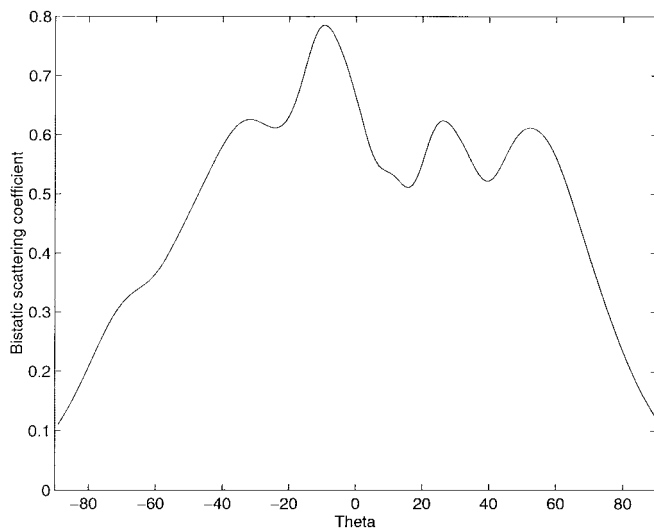


Fig. 7. Monte Carlo simulation: Copolarized bistatic scattering coefficient. A Gaussian beam is incident at  $\theta = -10^\circ$ .

Its size is  $3.9\lambda \times 3.9\lambda$ . The density of discretization is ten nodes per  $\lambda$ . Finest level blocks of size  $0.5\lambda \times 0.5\lambda$  are used, and the residual error stopping criterion for a transpose-free quasiminimal residual (TFQMR) [58] iterative solver is  $10^{-2}$ . The parameter  $B_{\text{di}}$  should be as small as possible for greatest efficiency. However,  $B_{\text{di}} = 1$  has been shown to be unsatisfactory in standard FMM's [34], while  $B_{\text{di}} = 2$  give very good results. For the SDFMM, we use  $B_{\text{di}} = 2$ , after ensuring that we have sufficiently accurate SDP integration rules for the given range of lateral displacements. A Gaussian beam lying in the  $x$ - $z$  plane and having no amplitude variation in the  $y$ -direction is used as the excitation. The beam is incident at an angle of  $10^\circ$  from the vertical with a positive  $x$ -component (i.e.,  $\theta = -10^\circ$ ). The half-width of the beam is  $W = L/4 = 0.975\lambda$ , and its electric field vector is polarized in the  $x$ - $z$  plane. The solution using the SDFMM produces a *current density* solution that is within 0.5% of that produced by solving the standard MoM. Fig. 6 depicts the RCS results, which are practically identical.

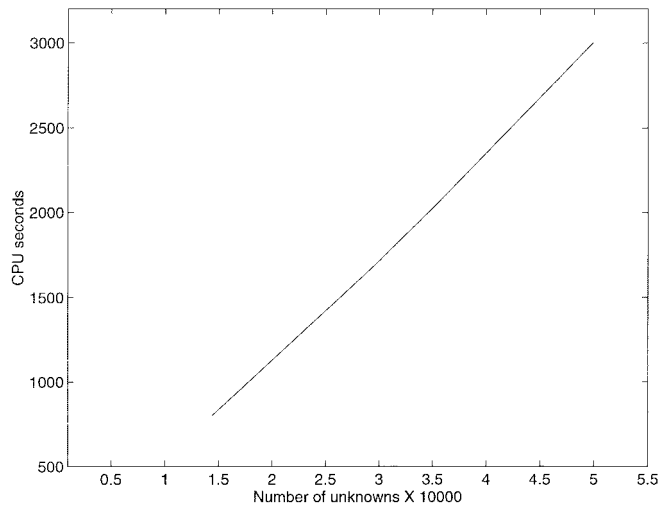


Fig. 9. Setup timings per surface.

A Monte Carlo simulation is carried out for an ensemble of 50 rough surfaces of size  $5.9\lambda \times 5.9\lambda$ , with  $\sigma = 0.5\lambda$  and  $l_c = 1.5\lambda$ . The excitation field is a Gaussian beam similar to the one in the above problem, with  $W = L/4 = 1.475\lambda$ . The problem involves  $N = 10325$  unknowns and requires approximately 52 h of CPU time for the complete simulation on a 60 MFlop SGI Power Challenge. The noncoherent bistatic scattering coefficients for the cross-polarized and copolarized cases are depicted in Figs. 7 and 8. Backscattering enhancement (at  $\theta = -10^\circ$ ) is clearly observed for both cases.

To verify the  $O(N)$  CPU time and memory estimates for the SDFMM, scaling tests are carried out using larger rough surfaces. The results of these tests are as follows. Setup times for rough surface computations, which include the computation of the near-field portion of the MoM matrix and the computation of plane wave expansions at the finest level, are depicted in Fig. 9. As suggested by the analysis in the previous section, the setup time scales approximately linearly with problem size. The CPU time for a matrix-vector product is shown in Fig. 10. The scaling of memory

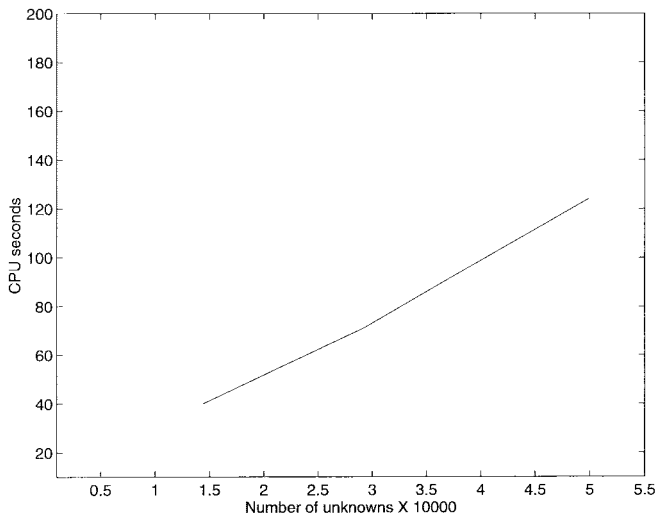


Fig. 10. Matrix-vector product timings.

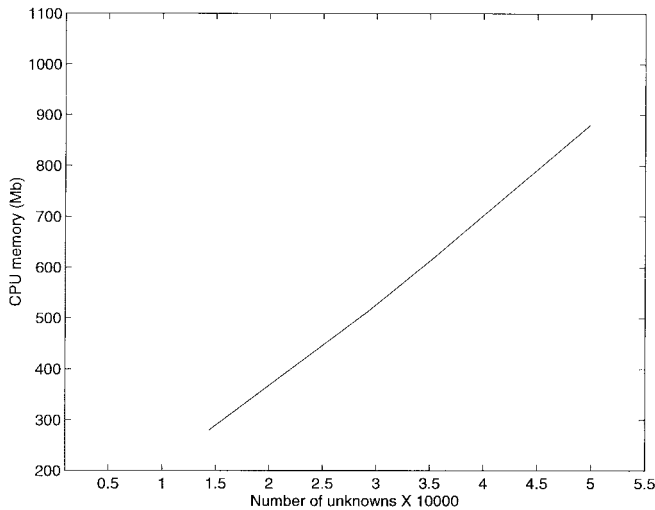


Fig. 11. Total memory requirements.

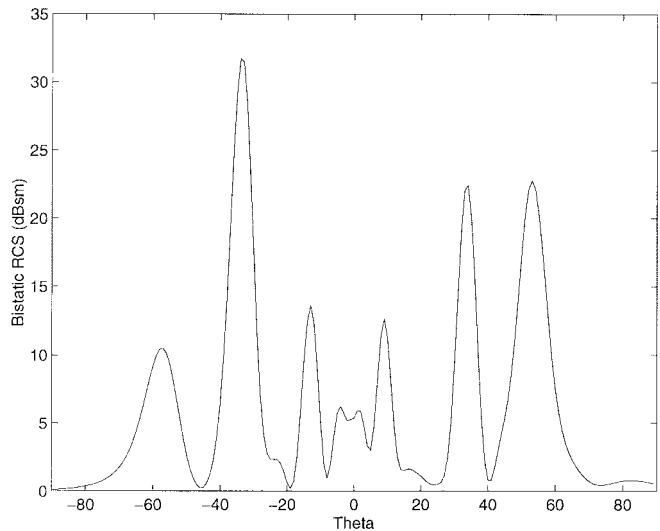
requirements is seen in Fig. 11. Both CPU time and memory scale approximately linearly, as predicted by the complexity analysis in the previous section.

Finally, the RCS of a  $420\lambda^2$  rough surface with  $\sigma = 0.3\lambda$  and  $l_c = 1.5\lambda$  is presented in Fig. 12. The surface was discretized using eight unknowns per  $\lambda$  resulting in approximately 80 000 unknowns. The excitation is similar to that used in the previous examples. This problem requires approximately 8 h of CPU time. A single matrix-vector product takes about 3 min.

## VII. CONCLUSION

A new multilevel algorithm, the SDFMM, has been developed to efficiently analyze scattering from quasiplanar structures. Gaussian, perfectly conducting rough surfaces have been used for illustration purposes in this work.

The proposed technique has  $O(N)$  CPU time and memory requirements and is rapid enough to permit Monte Carlo simulations of large surfaces in reasonable times. The technique is exact; the SDFMM solution can be made arbitrarily close to the MoM solution. For a fixed error tolerance  $\epsilon$ , the

Fig. 12. Bistatic RCS for a  $420\lambda^2$  rough surface with  $\sigma = 0.3\lambda$ .

computational cost is  $O(N \ln \epsilon^{-1})$ . A tradeoff exists therefore between accuracy and efficiency.

Further generalizations to the analysis of dielectric rough surfaces, anisotropic materials, and planar multilayered microwave circuits are currently under study. Efficient multilevel block-based preconditioners are also under development.

## REFERENCES

- [1] *Proc. Workshop Rough Surface Scattering Related Phenomena*, Napa Valley Lodge, Yountville, CA, 1996.
- [2] A. Ishimaru, *Wave Propagation and Scattering in Random Media*. New York: Academic, 1978.
- [3] E. Mendez, A. Navarrete, and R. Luna, "Statistics of the polarization properties of one-dimensional randomly rough surfaces," *J. Opt. Soc. Amer. A*, vol. 12, pp. 2507–2516, Nov. 1995.
- [4] A. Ishimaru, "Backscattering enhancement: From radar cross sections to electron and light localizations to rough surface scattering," *IEEE Antennas Propagat. Mag.*, vol. 33, pp. 7–11, Oct. 1991.
- [5] Y. Barabanenkov, Y. Kravtsov, V. Ozrin, and A. Saichev, "Enhanced backscattering: The universal wave phenomenon," *Proc. IEEE*, vol. 79, pp. 1367–1370, Oct. 1991.
- [6] A. Maradudin, A. McGurn, and E. Mendez, "Surface plasmon polariton mechanism for enhanced backscattering of light from one-dimensional randomly rough metal surfaces," *J. Opt. Soc. Amer. A*, vol. 12, pp. 2500–2506, Nov. 1995.
- [7] D. Maystre and M. Saillard, "Localization of light by randomly rough surfaces: Concept of localiton," *J. Opt. Soc. Amer. A*, vol. 11, pp. 680–690, Feb. 1994.
- [8] J. A. Kong, *Electromagnetic Wave Theory*. New York: Wiley, 1986.
- [9] E. Bahar and Y. Zhang, "A new unified full wave approach to evaluate the scatter cross sections of composite random rough surfaces," *IEEE Trans. Geosci. Remote Sensing*, vol. 34, pp. 973–980, July 1996.
- [10] E. Bahar, "Scattering cross sections for composite random surfaces: Full wave analysis," *Radio Sci.*, vol. 16, pp. 1327–1335, Nov. 1981.
- [11] M. El-Shenawee and E. Bahar, "Numerical method to compute TE and TM multiple scatter from rough surfaces exhibiting backscatter enhancement," *IEEE Trans. Magn.*, vol. 30, pp. 3140–3143, Sept. 1994.
- [12] E. Bahar and B. Lee, "Radar scatter cross sections for two-dimensional random rough surfaces—full wave solutions and comparisons with experiments," *Waves Random Media*, vol. 6, pp. 1–23, 1996.
- [13] R. E. Collin, "Scattering of an incident Gaussian beam by a perfectly conducting rough surface," *IEEE Trans. Antennas Propagat.*, vol. 42, pp. 70–74, Jan. 1994.
- [14] ———, "Electromagnetic scattering from perfectly conducting rough surface (a new full wave method)," *IEEE Trans. Antennas Propagat.*, vol. 40, pp. 1466–1477, Dec. 1992.
- [15] C. Vazouras, P. Cottis, and J. Kanellopoulos, "Scattering from conductive rough surface: A general perturbative solution," *IEEE Trans. Antennas Propagat.*, vol. 41, pp. 1232–1241, Sept. 1993.

- [16] E. Thorsos and S. Broschat, "An investigation of the small slope approximation for scattering from rough surfaces. Part I. Theory," *J. Acoust. Soc. Amer.*, vol. 97, pp. 2082–2093, Apr. 1995.
- [17] A. Benali, J. Chandezon, and J. Fontaine, "A new theory for scattering of electromagnetic waves from conducting or dielectric rough surfaces," *IEEE Trans. Antennas Propagat.*, vol. 40, pp. 141–148, Feb. 1992.
- [18] S. O. Rice, "Reflection of electromagnetic waves from slightly rounded surfaces," *Commun. Pure Appl. Math.*, vol. 4, pp. 351–378, 1951.
- [19] G. Valenzuela, "Depolarization of EM waves by slightly rounded surfaces," *IEEE Trans. Antennas Propagat.*, vol. AP-15, pp. 552–557, 1967.
- [20] J. C. Leader, "Bidirectional scattering of electromagnetic waves from rough surfaces," *Appl. Phys.*, vol. 42, pp. 4808–4816, 1971.
- [21] R. L. Wagner, J. Song, and W. Chew, "Monte Carlo simulation of electromagnetic scattering from two-dimensional random rough surfaces," *IEEE Trans. Antennas Propagat.*, vol. 45, pp. 235–245, Feb. 1997.
- [22] A. K. Fung, M. R. Shah, and S. Tjuatja, "Numerical solution of scattering from three-dimensional randomly rough surfaces," *IEEE Trans. Geosci. Remote Sensing*, vol. 32, pp. 986–994, Sept. 1994.
- [23] F. D. Hastings, J. B. Schneider, and S. L. Broschat, "A Monte-Carlo FDTD technique for rough surface scattering," *IEEE Trans. Antennas Propagat.*, vol. 43, pp. 1183–1191, Nov. 1995.
- [24] E. Michielssen, A. Boag, and W. C. Chew, "Scattering from elongated objects: Direct solution in  $o(n \log^2 n)$  operations," *Proc. Inst. Elect. Eng. Microw. Antennas Propagat.*, 1996, vol. 143, pp. 277–283.
- [25] R. Devayya and D. Wingham, "The numerical calculation of rough surface scattering by the conjugate gradient method," *IEEE Trans. Geosci. Remote Sensing*, vol. 30, pp. 645–648, May 1992.
- [26] P. Cao and C. Macaskill, "Iterative techniques for rough surface scattering problems," *Wave Motion*, vol. 21, pp. 209–229, 1995.
- [27] R. Chen and J. West, "Analysis of scattering from rough surfaces at large incidence angles using a periodic-surface moment method," *IEEE Trans. Geosci. Remote Sensing*, vol. 33, pp. 1206–1213, Sept. 1992.
- [28] L. Tsang, C. H. Chan, and H. Sangani, "Banded matrix iterative approach to Monte-Carlo simulations of scattering by large-scale random rough surface problems: TM case," *Electron. Lett.*, vol. 29, pp. 166–167, Jan. 1993.
- [29] L. Tsang, C. H. Chan, K. Pak, and H. Sangani, "Monte Carlo simulations of large-scale composite random rough-surface scattering based on the banded-matrix iterative approach," *J. Opt. Soc. Amer. A*, vol. 11, pp. 691–696, Feb. 1994.
- [30] D. A. Kapp and G. . Brown, "A new numerical method for rough-surface scattering calculations," *IEEE Trans. Antennas Propagat.*, vol. 44, pp. 711–721, May 1996.
- [31] K. Sarabandi, Y. Oh, and F. Ulaby, "A numerical simulation of scattering from one-dimensional inhomogeneous dielectric random surfaces," *IEEE Trans. Geosci. Remote Sensing*, vol. 34, pp. 425–432, Mar. 1996.
- [32] P. Tran and A. A. Maradudin, "The scattering of electromagnetic waves from a rough metallic surface," *Opt. Commun.*, vol. 110, pp. 269–273, Aug. 1994.
- [33] P. Tran, V. Celli, and A. A. Maradudin, "Electromagnetic scattering from a two dimensional, randomly rough, perfectly conducting surface: Iterative methods," *J. Opt. Soc. Amer. A*, vol. 11, pp. 1686–1689, May 1994.
- [34] J. Rahola, "Efficient solution of linear equations in electromagnetic scattering calculations," Center Sci. Comput., Espoo, Finland, Tech. Rep. CSC Res. Rep. R06/96, 1996.
- [35] A. Edelman, "Large dense numerical linear algebra in 1993: The parallel computing influence," *Int. J. Supercomput. Applicat.*, vol. 8, pp. 81–87, 1991.
- [36] L. Greengard, *The Rapid Evaluation of Potential Fields in Particle Systems*. Cambridge, MA: MIT Press, 1988.
- [37] C. R. Anderson, "An implementation of the fast multipole method without multipoles," *SIAM J. Sci. Stat. Comput.*, vol. 16, pp. 1082–1091, July 1992.
- [38] K. Nabors and J. White, "Fastcap: A multipole accelerated 3-D capacitance extraction program," *IEEE Trans. Computer-Aided Design*, vol. 10, pp. 1447–1459, Nov. 1991.
- [39] V. Jandhyala, E. Michielssen, and R. Mittra, "Multipole-accelerated capacitance computation for 3-D structures in a stratified dielectric medium using a closed form Green's function," *Int. J. Microw. Millimeter-Wave Comput.-Aided Eng.*, vol. 5, pp. 68–78, May 1995.
- [40] J. R. Phillips and J. K. White, "Precorrected-FFT methods for electromagnetic analysis of complex 3-D interconnect and packages," in *Progress Electromagn. Res. Symp.*–95, Seattle, WA.
- [41] V. Jandhyala, E. Michielssen, and R. Mittra, "A sparse multiresolution technique for fast capacitance computation," *Microw. Opt. Tech. Lett.*, vol. 11, pp. 242–247, Apr. 1996.
- [42] V. Rokhlin, "Rapid solution of integral equations of scattering theory in two dimensions," *J. Comput. Phys.*, vol. 36, pp. 414–439, 1990.
- [43] N. Engheta, W. D. Murphy, V. Rokhlin, and M. S. Vassiliou, "The fast multipole method (FMM) for electromagnetic scattering problems," *IEEE Trans. Antennas Propagat.*, vol. 40, pp. 634–641, June 1992.
- [44] R. Coifman, V. Rokhlin, and S. Wandzura, "The fast multipole method for the wave equation: A pedestrian description," *IEEE Antennas Propagat. Mag.*, vol. 35, pp. 7–12, June 1993.
- [45] C. C. Lu and W. C. Chew, "A multilevel algorithm for solving a boundary integral equation of wave scattering," *Microw. Opt. Tech. Lett.*, vol. 7, pp. 466–470, July 1994.
- [46] J. M. Song and W. C. Chew, "Multilevel fast-multipole algorithm for solving combined field integral equations of electromagnetic scattering," *Microw. Opt. Tech. Lett.*, vol. 10, pp. 14–19, Sept. 1995.
- [47] R. L. Wagner and W. C. Chew, "A ray-propagation fast multipole algorithm," *Microw. Opt. Tech. Lett.*, vol. 7, pp. 435–438, July 1994.
- [48] M. A. Epton and B. Dembart, "Multipole translation theory for the three-dimensional Laplace and Helmholtz equations," *SIAM J. Sci. Comput.*, vol. 16, pp. 865–897, July 1995.
- [49] C. C. Lu and W. C. Chew, "Fast algorithm for solving hybrid integral equations," *Proc. Inst. Elect. Eng. H*, 1993, vol. 140, pp. 455–460.
- [50] E. Michielssen and A. Boag, "A multilevel matrix decomposition algorithm for analyzing scattering from large structures," *IEEE Trans. Antennas Propagat.*, vol. 44, pp. 1086–1093, Aug. 1996.
- [51] C. H. Chan and L. S. Tsang, "A sparse-matrix canonical-grid method for scattering by many scatterers," *Microw. Opt. Tech. Lett.*, vol. 8, pp. 114–118, July 1995.
- [52] E. Bleszynski, M. Bleszynski, and T. Jaroszewicz, "A fast integral-equation solver for electromagnetic scattering problems," *IEEE APS Int. Symp. Dig.*, 1994, pp. 416–419.
- [53] R. L. Wagner, "Efficient computational techniques for electromagnetic propagation and scattering," Ph.D. dissertation, Univ. Illinois, Urbana-Champaign, 1996.
- [54] J. T. Johnson, L. Tsang, R. T. Shin, K. Pak, C. H. Chan, A. Ishimaru, and Y. Kuga, "Backscattering enhancement of electromagnetic waves from two-dimensional perfectly conducting random rough surfaces—a comparison of Monte Carlo simulations with experimental data," *IEEE Trans. Antennas Propagat.*, vol. 44, pp. 748–756, May 1996.
- [55] S. M. Rao, D. R. Wilton, and A. Glisson, "Electromagnetic scattering by surfaces of arbitrary shape," *IEEE Trans. Antennas Propagat.*, vol. AP-30, pp. 409–418, 1982.
- [56] G. Golub and C. van Loan, *Matrix Computations*. Baltimore, MD: Johns Hopkins Univ. Press, 1983.
- [57] Y. Saad, *Iterative Methods for Sparse Systems*, New York: PWS, 1996.
- [58] J. Volakis, "EM programmer's notebook," *IEEE Antennas Propagat. Mag.*, vol. 37, pp. 94–100, Dec. 1995.
- [59] W. C. Chew, *Waves and Fields in Inhomogeneous Media*. Piscataway, NJ: IEEE Press, 1995.
- [60] M. Abramowitz and I. Stegun, *Handbook of Mathematical Functions*. New York: Dover, 1965.
- [61] O. Bucci, C. Gennarelli, and C. Savarese, "Optimal interpolation of radiated fields over a sphere," *IEEE Trans. Antennas Propagat.*, vol. 39, pp. 1633–1643, Dec. 1991.



**Vikram Jandhyala** (S'93) was born on January 4, 1972, in New Delhi, India. He received the B.Tech. degree in electrical engineering from the Indian Institute of Technology, Delhi, in 1993, the M.S. degree in electrical engineering from the University of Illinois at Urbana-Champaign in 1995, and the Ph.D. degree from the University of Illinois at Urbana-Champaign in 1998.

He was a Graduate Research Assistant in the Electromagnetics Communication Laboratory, University of Illinois at Urbana-Champaign, from 1993 to 1995 and in the Center for Computational Electromagnetics, University of Illinois at Urbana-Champaign, from 1996 to March 1998. He is currently a Research and Development Engineer at Ansoft Corporation, Pittsburgh, PA. His current research interests are in the area of fast multilevel algorithms for analysis of electromagnetic scattering and for high-speed circuit parameter extraction.

Dr. Jandhyala is a recipient of the 1996–1997 IEEE MTT Graduate Fellowship and the 1998 Raj Mittra Outstanding Research Award, University of Illinois at Urbana-Champaign. He is a member of Phi Kappa Phi.



**Eric Michielssen** (M'95) received the M.S. degree in electrical engineering from Katholieke Universiteit Leuven (KUL), Leuven, Belgium, in 1987 and the Ph.D. degree from the University of Illinois at Urbana-Champaign in 1992.

He was a Research Assistant in the Microwaves and Lasers Laboratory, KUL, from 1987 to 1988. He joined the Faculty of the Department of Electrical and Computer Engineering, University of Illinois at Urbana-Champaign, as a Visiting Assistant Professor in 1992 and was appointed to his present position as Assistant Professor of Electrical and Computer Engineering in 1993. He is also currently the Associate Director of the Center for Computational Electromagnetics. His research interests include all aspects of computational electromagnetics, with a focus on fast multilevel algorithms, the application of combinatorial stochastic optimization techniques to the design of electromagnetic and optical components, and computational photonics.

Dr. Michielssen was appointed Belgian American Educational Foundation Fellow in 1988. He is a 1995 NSF CAREER award recipient. He serves as Associate Editor for *Radio Science* and was the Technical Chair for the 13th Annual Review of Computational Electromagnetics (ACES'97, Monterey, CA).



**Shanker Balasubramaniam** (M'96) received the B.Tech. degree in mechanical engineering from the Indian Institute of Technology, Madras, in 1989 and the M.S. and Ph.D. degrees from the Pennsylvania State University, University Park, in 1992 and 1993, respectively.

He was a Research Associate in the Department of Biochemistry and Biophysics, Iowa State University, Ames, from 1993 to 1996, where he worked on molecular theories of optical activity. Since 1996, he has been with the Center for Computational Electromagnetics, University of Illinois at Urbana-Champaign. He has published 25 journal articles and a number of conference papers. His research interests include all aspects of computational electromagnetics and electromagnetic wave propagation through complex media.



**Weng Cho Chew** (S'79-M'80-SM'86-F'93) was born on June 9, 1953, in Malaysia. He received the B.S. degree in 1976, both the M.S. and Engineer's degrees in 1978, and the Ph.D. degree in 1980, all in electrical engineering, from the Massachusetts Institute of Technology, Cambridge.

He was with Schlumberger-Doll Research, Ridgefield, CT, from 1981 to 1985. While he was there, he was a Program Leader and later a Department Manager. From 1985 to 1990, he was an Associate Professor with the University of Illinois at Urbana-Champaign. From 1989 to 1993, he was the Associate Director of the Advanced Construction Technology Center, University of Illinois at Urbana-Champaign. He is now a Professor at the University of Illinois at Urbana-Champaign, teaching graduate courses in Waves and Fields in Inhomogeneous Media and Theory of Microwave and Optical Waveguides and supervising a graduate research program. He is also the Director of the Center for Computational Electromagnetics and the Electromagnetics Laboratory at the same university. His name is often listed in the List of Excellent Instructors on campus. He has authored a book, *Waves and Fields in Inhomogeneous Media*, Piscataway, NJ: IEEE Press, 1995, published over 110 scientific journal articles, and presented over 130 conference papers. His recent research interest has been in the areas of wave propagation, scattering, inverse scattering, and fast algorithms related to scattering, inhomogeneous media for geophysical subsurface sensing, and nondestructive testing applications. Previously, he has also analyzed electrochemical effects and dielectric properties of composite materials, microwave and optical waveguides, and microstrip antennas.

Dr. Chew is a member of Eta Kappa Nu, Tau Beta Pi, URSI Commissions B and F, and an active member with the Society of Exploration Geophysics. He was an NSF Presidential Young Investigator for 1986. He was also an AdCom member and is presently an Associate Editor of the IEEE TRANSACTIONS ON GEOSCIENCE AND REMOTE SENSING. He was also an Associate Editor of the *International Journal of Imaging Systems and Technology* and has been a Guest Editor of *Radio Science* and the *International Journal of Imaging Systems and Technology*.